Fuel Processing Technology 212 (2021) 106633

Contents lists available at ScienceDirect

Fuel Processing Technology

journal homepage: www.elsevier.com/locate/fuproc

Research article

Supercritical extraction and microwave activation of wood wastes for enhanced syngas production and generation of fullerene-like soot particles

Anna Trubetskaya[a,*], Andrew J. Hunt[b], Vitaliy L. Budarin[c], Thomas M. Attard[c], Jens Kling[d], Gerrit R. Surup[e], Mehrdad Arshadi[f], Kentaro Umeki[g]

[a] Department of Chemical Sciences, University of Limerick, Limerick, Ireland
[b] Materials Chemistry Research Center, Department of Chemistry and Center of Excellence for Innovation in Chemistry, Faculty of Science, Khon Kaen University, 123 Mittraparb Road, 40002 Khon Kaen, Thailand
[c] Department of Chemistry, The University of York, Heslington, York YO10 5DD, UK
[d] Center for Electron Nanoscopy, Technical University of Denmark, 2800 Kgs. Lyngby, Denmark
[e] Department of Materials Science and Engineering, Norwegian University of Science and Technology, 7491 Trondheim, Norway
[f] Department of Forest Biomaterials and Technology, Swedish University of Agricultural Sciences, 90183 Umeå, Sweden
[g] Energy Science Division, Luleå University of Technology, 97187 Luleå, Sweden

ARTICLE INFO

Keywords:
Biomass
Pyrolysis
Gasification
Carbon dioxide
Biorefinery
Nanomaterials

ABSTRACT

This work demonstrated that supercritical carbon dioxide extraction is effective as a pre-treatment technology to generate soot particles with the fullerene-like structure and increase syngas yield from extracted residues during coupled microwave activation with gasification. Supercritical carbon dioxide extraction removes over half of the fatty and resin acids from needles and branches, whereas the extraction of needles generates greater yields of value-added compounds. The high yields of extractives indicate the effective conversion of waste wood for the sustainable production of value-added chemicals. The wood extraction did not influence the solid residue yields during pyrolysis/gasification emphasizing the significant potential of integrating the extraction process into the holistic biorefinery. Interestingly, supercritical carbon dioxide extraction had a significant effect on the structure and quality of soot particles formed. The differences in the extractives composition led to the formation of needle soot particles with a porous and less ordered nanostructure, whereas the soot branches obtained a ring graphitic structure. The greater yields of steroids and terpenes during the extraction of needles compared to the branches pretreatment indicated the influence of the extractives type on the soot nanostructure.

1. Introduction

Biomass is a renewable and widely available resource that can be used for heat, power, as a feedstock for liquid fuels and as a sustainable chemical production [1]. The cost-efficient development of biorefineries depends on feedstock flexibility and effective pre-treatment processes for chemical production in combination with efficient power and heat generation [2]. The pre-treatment processes decrease the water content in feedstock, increase energy density, and generate high value-added products for the chemical industry. Remaining solid fuel fractions are used for the generation of renewable and clean energy. Little is known about the effect of supercritical CO_2 ($scCO_2$) extraction on the yields and properties of products from high-temperature pyrolysis and gasification.

In the forestry sector, utilizing the supercritical extraction process has been shown to improve the off-gassing of wood pellets, thus reducing the potential for uncontrolled auto-oxidation, while maintaining pellet properties [3,4]. Moreover, supercritical CO_2 extraction can also improve the physicochemical properties of solid char from pyrolysis at high temperatures, leading to greater electric conductivity and low reactivity of solid char [5]. Supercritical CO_2 extraction increases the bending strength and stiffness of residual wood and thus, decreases the cost of process scaling up, wood storage and transportation [6]. Several methods exist for the extraction of high-value molecules from biomass including conventional organic solvent extraction, hydrodistillation, low-pressure solvent extraction and hydrothermal feedstock processing [7–9]. Supercritical fluids demonstrate properties between those of a liquid and a gas, with the viscosity of a supercritical fluid being an order of magnitude lower than a liquid, whereas the diffusivity is an order of magnitude higher and thus, leading to the enhanced heat and mass transfer [10]. The properties of a solvent can be fine-tuned by varying the temperature and pressure. Conventional

* Corresponding author.
E-mail address: anna.trubetskaya@ul.ie (A. Trubetskaya).

https://doi.org/10.1016/j.fuproc.2020.106633
Received 12 May 2020; Received in revised form 22 August 2020; Accepted 2 October 2020
Available online 15 October 2020

solvents traditionally utilized in wax extraction (such as hexane) are frequently viewed as being problematic due to the toxicological and environmental impacts [11]. Supercritical fluid extraction using CO_2 as a solvent has an easily accessible critical point, is non-flammable, has minimal toxicity and is widely available [12]. Supercritical CO_2 extraction has been conducted on a commercial scale for over two decades for the extraction of products from biomass [13]. Thus, the proposed biorefinery concepts [14–16], which combine the $scCO_2$ extraction and pyrolysis processes, will be considered in the present work for the use of low value-added forestry residues for the cost-efficient production of extracted value-added products and remaining solid feedstock for further use in the production of bio-oil using microwave pyrolysis and syngas using fast pyrolysis [17,18].

The advantage of pyrolysis is that the yield of end-products can be altered depending on the operating conditions, whereas the heat treatment temperature and the heating rate are known to have most influence on the product yield and composition [19,20]. The combination of $scCO_2$ extraction process with microwave pyrolysis has been rarely studied in the literature. However, microwave pyrolysis has been previously shown to be an energy efficient process for biomass conversion and has become widely accepted as a mild and controllable processing tool [21]. Microwave pyrolysis has been carried out at temperatures below 350°C due to the high pyrolysis rates, good energy efficiency and better controllability than conventional pyrolysis [22,23]. Microwave pyrolysis converts biomass into high-quality bio-oil for chemicals and solid char that is a valuable feedstock for heat and power generation [24]. The combination of a low temperature microwave pyrolysis with $scCO_2$ extraction could provide better control over the biomass decomposition and a better separation of undesirable water and water-soluble components in the bio-oil and thus get closer to fuel-ready oils than what has previously been achieved. Moreover, the combination of supercritical carbon dioxide extraction with microwave pyrolysis will improve the total process efficiency due to the low solid product yields and the better quality of bio-oil [24].

Forest industry produces millions of tons of waste wood residues which are ideally suited for exploitation by a combination of green technologies for the generation of value added products. Wood chemical composition varies with tree part (root, stem, or branch), type of wood, geographic location, climate and soil conditions [25]. The mineral content and distribution of lignocellulosic compounds show significant variations between tree parts (needles, branches, stem, bark, etc.) [26]. Spruce needles have high phosphorus, sulfur, potassium and calcium contents, whereas the spruce bark contains high amounts of calcium and magnesium [27,28]. The ash and extractives contents are higher in pinewood bark compared to stemwood [29], whereas branches and root samples contain more minerals, galactan, xylan and lignin compared to glucomannan rich stemwood [30]. Compared to wood, needles are richer in extractives, especially waxes [31,32]. A recent study has demonstrated that supercritical carbon dioxide extraction had little impact on the physical properties of original wood nor on the yield of solid char using conventional pyrolysis. Importantly, a mixture of different low quality wood fractions was able to yield chars with reactivity and dielectric properties approaching that of fossil-based metallurgical coke [33]. However, the effect of supercritical carbon dioxide extraction on the properties of liquid products and gas in the conventional pyrolysis and products from fast pyrolysis at temperatures greater than 900°C has been rarely studied. Microwave heating of biomass and organic wastes creates challenges due to the poor microwave adsorbance of various carbon materials leading to an incomplete conversion, and thus, high yields of solid char in pyrolysis [34,35]. The remaining char from the microwave pyrolysis has a potential to be used as a feedstock in the combustion and gasification processes [36]. In the present study, the properties of solid char from microwave pyrolysis using remaining solid feedstock after $scCO_2$ extraction were further tested in the entrained flow gasification reactor [37,38].

Forest industry produces millions of tons of waste wood residues which can be used in a closed loop efficient process. Supercritical extraction followed by biomass microwave pyrolysis has a high potential to remove extractives and other volatile compounds, and thus, to produce a high quality bio-oil and value-added feedstock for gasification and combustion. Understanding the properties of wood fractions (bark, stem, needles, branches) is important for: (1) optimizing solvent extraction processes leading to maximal yields of extractives and (2) optimizing the char yield in high-temperature processes. To the author's knowledge, no previous work has been carried out on the characterization of solid char from microwave pyrolysis for the use in fast pyrolysis as a pre-step for gasification and combustion. The main objective of this work is to demonstrate that the removal of extractives from low value forest residues using $scCO_2$ treatment provides both an added-value product for the chemical industry as well as yielding a valuable feedstock for the production of char in microwave pyrolysis and fast pyrolysis for the energy sector.

2. Materials and methods

On average, 147 year old Scots pine trees in northern Sweden were harvested from a forest stand. Fractions from harvested trees were green needles, and branches without needles. Prior to the $scCO_2$ extraction and microwave pyrolysis, wood fractions were comminuted on a hammer mill (MAFA EU-4B manufacturer) with an operating speed of 60 Hz. $ScCO_2$ extraction was performed on different pinewood fractions. Solid residues were collected after extraction and dried at room temperature. The extractives were collected and weighed for the calculation of yields. The composition of volatiles in non-treated wood fractions and samples after $scCO_2$ extraction was investigated by pyrolysis-gas chromatography/mass spectrometry (Py-GC/MS). The branches after CO_2 extraction were pyrolyzed in the microwave furnace, whereby the char and bio-oil yields were measured. The collected char was further reacted at 1100°C in the drop tube furnace (DTF) under pyrolysis and CO_2 gasification conditions. Soot nanostructure and particle size were studied using microscopy. The effects of $scCO_2$ extraction and fast pyrolysis conditions on the wood char and soot reactivity were investigated using a thermogravimetric analyzer.

2.1. Supercritical CO_2 extraction

The $scCO_2$ extractions were conducted using a supercritical extractor SFE 500 (Thar technologies, USA). Supercritical fluid grade carbon dioxide (99.99%, dip-tube liquefied CO_2 cylinder obtained from BOC) was used in the extractions. The CO_2 supplied from a cylinder as a liquid was maintained in this state through a cooling unit (−2°C) to avoid cavitation in the high pressure pump. $ScCO_2$ extractions of the different biomass types were optimized using a two-level factorial design [3]. Evaluation was made by determination of the extracts' weight in the different experiments. Approximately 180 g of biomass was placed into the 500 mL extraction vessel. The reaction vessel was heated to the required temperature and was equilibrated for 5 min. An internal pump was used in order to obtain the required pressure. The system was run in a dynamic mode, in which the carbon dioxide containing the extractives flowed into the collection vessel. A flow rate of 40 g min^{-1} of liquid CO_2 was applied and the extraction was carried out for 2 h. On completion the system was depressurized over a period of 60 min. The conditions chosen (400 bar and 60°C) for the $scCO_2$ extraction of the needles and branches were based on optimisation studies in the literature [39]. Pressure and temperature are known to be related to density of CO_2 that needs to be incorporated in order to maximise the % crude extract [40]. The conditions chosen (400 bar and 60°C) for the $scCO_2$ extraction are the optimal conditions leading to the highest extraction rates [33].

2.2. Microwave pyrolysis

Fifty gram of $scCO_2$ extracted branches were weighed and exposed to a maximum microwave power of 1200 W using a rotative solid phase microwave reactor ROTO SYNTH (Milestone, Italy) fitted with a vacuum module VAC 2000 in series. The sample was heated at a rate of 17 °C min^{-1} to a maximum temperature of 180°C. Based on previous work [5,41], the heating rate and the heat treatment temperature were selected to obtain the maximal yield of liquid fractions and to minimize the char yield. Liquid fractions were collected via the vacuum unit that collected and condensed vapours during pyrolysis. The char yield was determined by weighing the sample before and after microwave treatment, as discussed by Budarin et al. [24].

The liquid products collected by the condensers from the microwave pyrolysis were rinsed with dichloromethane (DCM), as described in the previous work [37,42]. The oil fraction in the liquid mixture was separated out and concentrated to a detection level using a Genevac Rocket Evaporation system. The oil fraction composition was then determined using a Varian CP-3800 GC coupled with a Varian Saturn 2200 mass spectrometer (MS). The conditions for the GC/MS equipment were: GC injector port temperature 290°C; transfer line temperature 280°C; manifold temperature 120°C and trap temperature 200°C; the oven program temperature was 40°C for 2 min, then it was ramped to 280°C with 5°C min^{-1}, and finally held at 280°C for 10 min. The compounds in the oil were quantified using external standards.

2.3. Fast pyrolysis in drop tube reactor

The feedstock was reacted at 1100°C in a laminar drop tube reactor. The DTR setup was described in detail by Trubetskaya et al. [43] and shown in Fig. 1. Based on previous work [44], operation at 1100°C was selected to simulate the operating conditions in an industrial-scale entrained-flow gasifier. The reactor consists of an alumina tube (internal diameter: 54 mm, heated length: 1.06 m) heated by four heating elements with independent temperature control. Gas flow rate into the reactor is regulated by mass flow controllers (EL-FLOW® Select, Bronkhorst High-Tech B.V.). The feeding system is based on a syringe pump that displaces a bed of fuel that falls directly into the high temperature zone in the reactor through a water-cooled probe. The syringe pump was vibrated to ensure stable feeding of the fuel particles. In each experiment, ≈ 5 g of biomass or char was fed into the reactor at a rate of 0.2 g min^{-1}. Both primary (0.18 L min^{-1} measured at 20°C and 101.3 kPa) and secondary (4.8 L min^{-1} measured at 20°C and 101.3 kPa) feed gases were N_2. The residence time of fuel particles was estimated to be about 1 s, taking into account density changes during pyrolysis. Reaction products were separated into coarse particles (mainly char and fly ashes), fine particles (mainly soot and ash aerosols), permanent gases, and tars. Coarse particles were captured in a cyclone (cut size 2.5μm). Soot particles exited the cyclone and were collected on a grade QM-A quartz filter with a diameter of 50 mm (Whatman, GE Healthcare Life Science).

The carbon and hydrogen balances using the experimental data of yields and composition of gas and solid products represent an average of two measurements, as described in the previous work [20,45]. Solid products were categorized as char, soot, and coke. Char and soot were collected in a char bin and on a filter, respectively. Char is the fraction of non-devolatilized solid present in the initial biomass, consisting mainly of carbon and ash. Coke, the carbonaceous material deposited on the reactor walls, was quantified after each experiment by measurement of the concentration of CO_2 during oxidation. Water, vapor, tars, and large hydrocarbon yields (organics + vapor) were not measured directly, instead estimated by gravimetric differences.

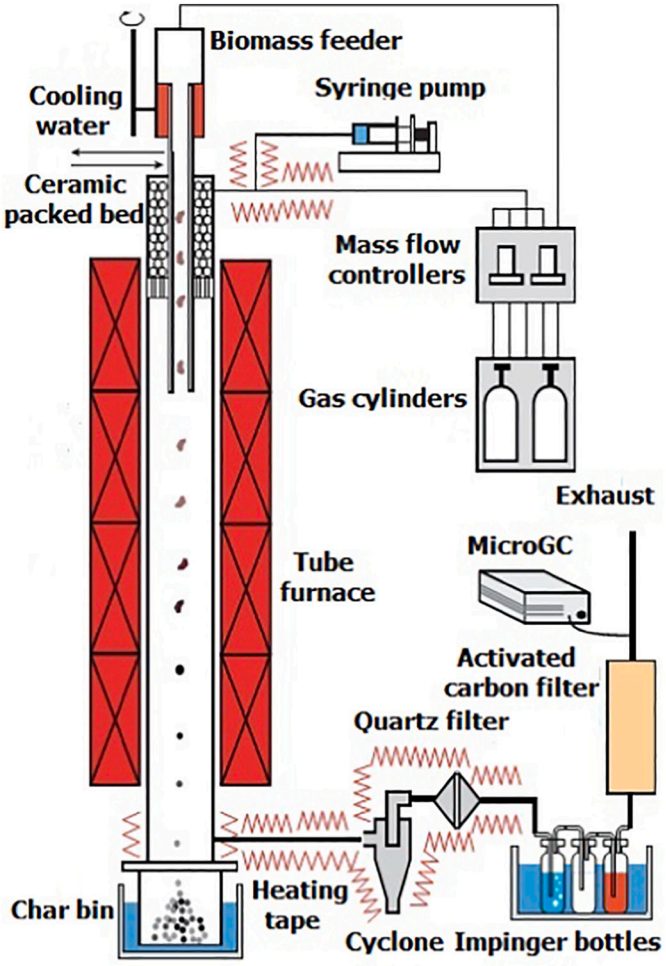

Fig. 1. Schematic view of the drop tube reactor implemented in this study.

2.4. Product characterization

2.4.1. Elemental analysis

The elemental analysis was performed on an Analyzer Series II (Perkin Elmer, USA), according to the procedure described in ASTM D5373–02. Acetanilide was used as a reference standard. The oxygen content was calculated by difference.

2.4.2. Proximate analysis

The proximate analysis was conducted to determine the contents of moisture, ash, volatiles, and fixed carbon according to the procedures described in ASTM D2216–19, ASTM D1102–84, ASTM D3175–11, and ASTM D3172–13. The high heating value was determined by the bomb calorimeter (IKA C-200) according to the procedure described in ASTM D2015–85.

2.4.3. Ash compositional analysis

The ash compositional analysis was performed by ICP-OES in ASTM D6349–13. Prior to the analysis, biomass samples were pre-heated in oxygen at 10°C min^{-1} up to 550°C and kept at that temperature for 7 h.

2.4.4. Thermogravimetric analysis

The char samples from the microwave treatment and the char and soot samples from the further high-temperature pyrolysis and CO_2 gasification in the drop tube reactor were firstly crushed to a fine powder in a mortar with a ceramic pestle. The thermal decomposition of samples was determined using a thermogravimetric instrument STARe System (Mettler Toledo, USA) by loading 5 mg of sample in Al_2O_3

crucible.

The initial sample mass and heating rates used in the TG experiments were selected to minimize possible mass transfer limitations that may occur by O_2/CO_2 gasification concentration gradients through the TG crucible down to the particle bed, through the particle bed, and inside the soot and char particles [46,47]. The previous results [48] showed that less than 5 mg of char and soot samples should be applied to avoid mass transfer limitations using a heating rate of 10°C min^{-1} in 40% volume fraction CO_2 gasification. The kinetic parameters of char and soot samples were derived by the integral method presented by Coats and Redfern [49]. Through integral transformation and mathematical approximation, the linear equation was expressed in the form:

$$\ln\left(-\frac{\ln(1-X)}{T^2}\right) = \ln\left(\frac{A\cdot R}{\kappa\cdot E_a}\right) - \frac{E_a}{R\cdot T} \quad (1)$$

In Eq. (1), κ is the heating rate and R is the gas constant. A plot of ln $(-\ln(1\text{-}X)\ T^{-2})$ versus T^{-1} gives a straight line whose slope and intercept determine the values of the activation energy (E_a) and pre-exponential factor (A). The previous results [20,50] showed that a first order reaction model in both solid residue mass and gasification agent can describe the experimental results well.

2.5. Feedstock characterization

2.5.1. Py-GC/MS

The Py-GC/MS analysis was conducted on non-treated needles and branches and samples after $scCO_2$ extraction using a Trapping Pyrolysis Autosampler 5250-T (CDS Analytical, UK) coupled to a gas chromatography unit 7890 (Agilent Technologies, USA) and a mass spectrometer 5977A (Agilent Technologies, USA). Twenty milligram of wood samples was loaded into a quartz tube and pyrolyzed at 600°C for 10 s. The pyrolysate was separated on a 30 m length, 0.25 mm internal diameter and 0.25 μm film thickness capillary column DB-5 (Agilent Technologies, USA). The GC was operated at a constant helium flow of 1 mL min^{-1} and a 50:1 split ratio. The GC inlet and detector temperatures were both 350°C. The oven program started at 40°C for 2 min and was heated up to 300°C at a constant heating rate of 10 K min^{-1} with a final hold time 30 min. The mass spectrometer ion source was set to 230°C and the interface to 280°C, scanning took place once per second in the range of 50 to 550 *m/z*. Volatile compounds were identified by comparing the mass spectra with NIST Lab database versions 147 and 27 with an identity threshold cut-off of 50. Py-GC/MS experiments were conducted at least in duplicate. More than 130 peaks were displayed on the chromatograms. The major target compounds with a spectral match quality greater than 85% were listed in the supplemental material (Table S-1). The chromatographic signals were integrated and the relative peak areas were calculated. The calculation of total peak area included the identified and unknown compounds in pyrolysis.

2.5.2. TG-FTIR

The temperature resolved composition of volatiles was characterized using a FTIR spectrometer EGA TL 8000 (Perkin-Elmer, USA) coupled to the thermogravimetric analyzer. For the TG-FTIR analysis, ca. 10 mg of a sample and high purge gas flow rates (100 ml min^{-1}) were used in order to optimize the FTIR signal. The wood samples were evenly dispersed on ceramic crucibles, pre-dried at 105°C and heated up to 600°C at a constant heating rate of 10°C min^{-1}. The FTIR instrument equipped with a deuterated triglycine sulfate (DTGS) detector was set to a scan rate of 0.2 cm s^{-1} and to a resolution of 2 cm^{-1} in the 4000–450 cm^{-1} range. Thus, 288 spectra were acquired every 10 s during the heating ramp. The temperatures of the sampling line and the gas cell were kept at 230°C. The pump of the FTIR system constantly extracted 50 mL min^{-1} from the TGA off-gas through the FTIR gas cell. The spectra interpretation of smaller compounds (H_2O, CH_4, CO_2 and CO) were identified, assigned and recorded according to the characteristics adsorption data in Table 1. The larger compounds were only grouped and assigned to corresponding bands of adsorption.

Table 1
Absorption bands and specific wave numbers used for the gas profiles [51].

Compound	Absorption band, cm^{-1}	Identification, cm^{-1}
H_2O	4000–3400, 1800–1300	3853
CH_4	3018	3018
CO_2	2391–2217	2360
CO	2220–2150, 2140–2060	2186

2.6. Soot characterization

2.6.1. Soot pretreatment for microscopy

Prior to microscopy, soot samples were kept at 350°C for 4 h in a thermogravimetric instrument to reduce the volatile contents. Samples were dry dispersed on a lacey carbon copper grid.

2.6.2. Transmission electron microscopy

Soot morphology was studied using a FEI Titan transmission electron microscope operated at 120 keV.

2.6.3. Particle size distribution analysis using TEM

The particle size of soot samples was estimated manually from TEM images using the ImageJ software [52,53]. Only clearly visible primary particles were selected for accurate analysis. The data was assessed to establish particle size distributions. For size analysis, soot particles were assumed spherical. Particle size analysis was conducted on 100 particles at each operating condition. Standard deviation was calculated for curvature, fiber length (see definition below) and separation distance of graphene layers as described in the supplemental material (Eq. (1)). The curvature of a single graphene sheet was calculated as shown in the supplemental material (Eq. (2)).

3. Results and discussion

3.1. Biomass characterization

Fuel selection in this study was based on the differences in the ash composition and plant cell compounds (cellulose, hemicellulose, lignin, extractives). The proximate, ultimate and ash compositional analysis of non-treated wood fractions and samples after $scCO_2$ extraction is shown in Table 2. The compositional analysis of biomass (cellulose, hemicellulose, acid-soluble lignin, acid-insoluble lignin, protein and extractives) was conducted according to NREL technical reports [54–56] and Thammasouk et al. [57], and shown in Table 3.

3.2. Product yields in DTF

The mass balances of needles and branches pyrolysis with respect to measured solid residues (char, soot, coke) and major gaseous products (CO_2, H_2, CO, CH_4, C_2H_4, C_2H_2) are shown in Fig. 2(a). During pyrolysis of needles and branches, mainly gaseous products were formed, along with smaller amounts of solid residues. Almost all hydrogen (> 95%) was found in the form of gaseous products. The differences in product yields of non-treated wood fractions and $scCO_2$ extracted samples were small. The removal of extractives increases the temperature of hemicellulose and cellulose decomposition only slightly, leading to the reduced influence of supercritical CO_2 extraction on the total char yield during fast pyrolysis at high temperatures [58]. Moreover, the thermogravimetric analysis showed that the char yield from the pyrolysis of extractives was as high as 36% which is similar to the char yields from the pyrolysis of organosolv lignin [59,60].

Table 2
Proximate, ultimate and ash analyses of non-treated Scots pinewood fractions and samples after $scCO_2$ extraction.

Fuel	Needles		Branches	
	Original	$scCO_2$ extracted	Original	$scCO_2$ extracted
	Proximate and ultimate analysis (% on dry basis)			
Moisture[a]	6.5	5.6	7.3	6.8
Ash (550 °C)	2.2	2.3	0.8	1
Volatiles	80.8	78.8	80.6	70.9
HHV[b]	22.4	21.3	21.7	20.9
LHV[b]	21	20	20.4	19.6
C	53.7	51.8	53.5	51.4
H	6.5	6.3	6.2	5.9
O	36.1	38.2	39.0	41.2
N	1.3	1.4	0.4	0.5
S	0.1	0.1	0.03	0.04
	Ash compositional analysis (mg kg^{-1} on dry basis)			
Cl	0.02	0.02	< 0.01	0.01
Al	250	200	150	200
Ca	2450	2500	1300	1200
Fe	70	70	60	70
K	5600	5500	2000	1900
Mg	750	800	400	400
Na	25	20	< 10	10
P	1500	1550	400	400
Si	400	380	400	350
Ti	4	3	6	10

[a] wt% (as received)
[b] in MJ kg^{-1}.

Table 3
Composition of non-treated Scots pinewood fractions and extractives yield after $scCO_2$ extraction, calculated in percentage based on dry basis (wt%).

Biomass	Cellulose	Hemicellulose	Lignin		Extractives	
			Acid insoluble	Acid soluble	(raw wood)	(after $scCO_2$ extraction
Needles	23.4	15.1	26.5	0.5	12.1	7.9
Branches	25.3	19.4	28	1	8	4.4

The yield of aldehydes and alkanes formed during pyrolysis of extractives was also similar to the yields from original wood pyrolysis, whereas the gas yield was lower during the decomposition of extractives than in wood pyrolysis [60]. Fig. 2(b) illustrated the mass balances of microwave treated char of $scCO_2$ extracted species in pyrolysis and CO_2 gasification, with the gas yield remaining greater in CO_2 gasification than in pyrolysis due to the homogeneous reaction between CO_2 and volatiles [61]. Fig. 3 illustrates the soot and char yields which are separated into organic matter and ash. The soot yield remained only slightly changed with the supercritical CO_2 extraction, whereas the char yield of branches and needles decreased by approximately 4 and 3% respectively in pyrolysis. Supercritical CO_2 extraction also led to the decrease in the inorganic matter content of needles and char branch samples. The char yield of $scCO_2$ extracted char branches using microwave pre-treatment was lower in CO_2 gasification than during fast pyrolysis in the drop tube reactor, whereas greater soot yield was obtained in CO_2 gasification, confirming the previous results of Umeki et al. [62]. In general, during high-temperature fast pyrolysis the soot yield of $scCO_2$ branches from additional treatment using the microwave pyrolysis was lower than the soot yield from $scCO_2$ extracted branches, as shown in Fig. 3(b).

The pyrolysis and gasification experiments showed that $scCO_2$ extraction of wood fractions increased syngas yield and had a negligible influence on the solid product yields, as shown in Fig. 2(a) and supplemental material (Fig. S-3(a)). The $scCO_2$ extraction removed most of

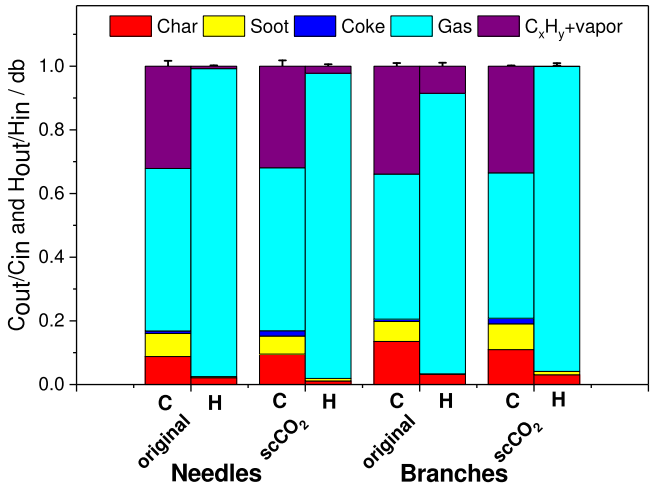

(a): Needles and branches

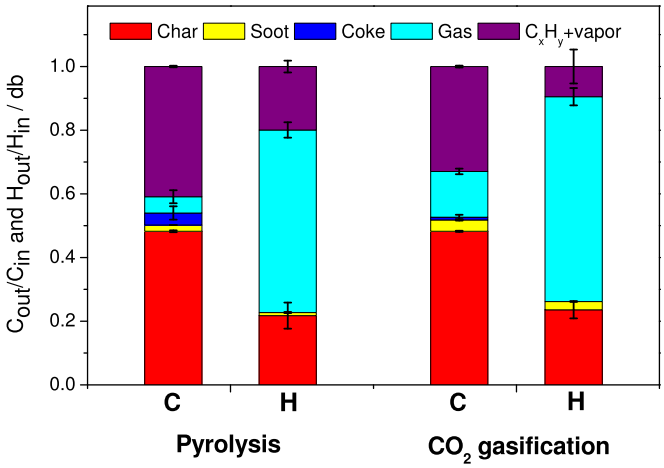

(b): Pyrolysis and gasification of $scCO_2$ extracted branches

Fig. 2. Carbon and hydrogen distribution of: (a) needles and branches and samples after $scCO_2$ extraction and (b) from pyrolysis and CO_2 gasification of $scCO_2$ branches char that was prior treated in the microwave reactor (relative to microwave char).

the resin acids, aromatics and steroids from the wood fraction. Extracted components are more thermally stable and less reactive than the majority of volatile compounds, which lead to the increased yield of syngas during CO_2 gasification. The concentrations of H_2, CO, CO_2 and C_xH_y (CH_4, C_2H_2, C_2H_4) from pyrolysis and gasification are shown in the supplemental material (Fig. S-3(b)). The non-treated branches and $scCO_2$ extracted sample had a greater concentration of H_2 and CO than needles which contained less cellulose and lignin than branches. Cellulose, with more carbonyl and carboxyl groups, accounted for a greater CO yield, whereas lignin with more methoxylated aromatic ring structures released more H_2 and CH_4 in pyrolysis [63]. Supplemental material (Fig. S-3) shows that $scCO_2$ extraction led to the greater gas yield with the increased CO_2 and CO formation in needles and branches pyrolysis. The removal of extractives from pinewood enhanced the formation of acetic acid and levoglucosan due to the changes in cellulosic fiber orientation [64]. The char yield of microwave char reacted in pyrolysis was slightly greater than the char yield in CO_2 gasification. Compared with pyrolysis of $scCO_2$ extracted microwave char, the concentration of CO was significantly greater and the concentration of H_2 was slightly lower in CO_2 gasification, as shown in the supplemental material (Fig. S-3). The char yield in CO_2 gasification decreased due to

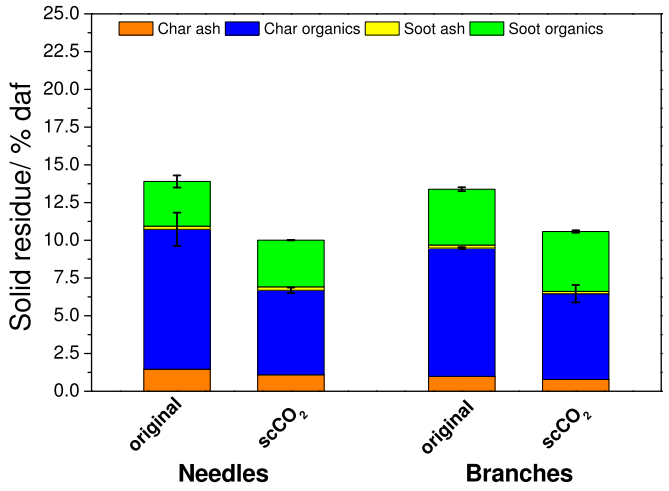

(a): Needles and branches

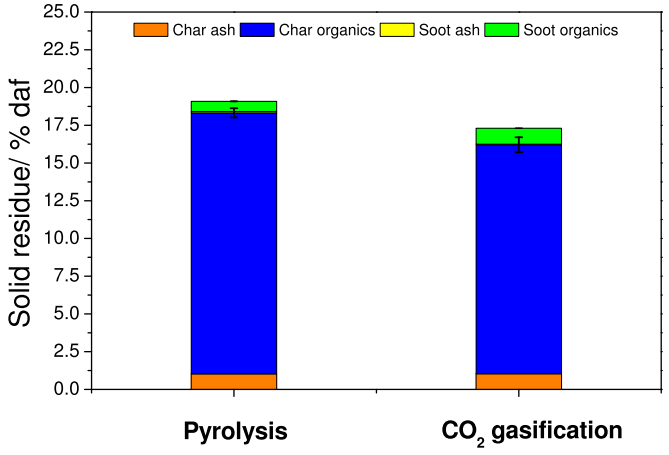

(b): Pyrolysis and gasification of $scCO_2$ extracted branches

Fig. 3. Soot and char yields (wt% relative to original feedstock) from pyrolysis of: (a) needles and branches and samples after $scCO_2$ extraction) and (b) from pyrolysis and CO_2 gasification of $scCO_2$ branches char that was prior treated in the microwave reactor. The total yield of soot and char is separated in ash and organic matters. The error bars characterize the deviations between the total yields of the char and soot.

the heterogeneous Boudouard reaction (Eq. (5)), whereas the reaction between solid carbon and CO_2 increased the formation of CO. Likewise, the H_2 concentration decreased due to the water-gas-shift reaction (Eq. (4)) at temperatures above 1100°C and at residence time less than 3 s, confirming the previous results [65,66].

Dry reforming: $C_nH_m + nCO_2 \rightarrow 2nCO + \left(\frac{m}{2}\right)H_2$ (2)

Steam reforming: $C_nH_m + nH_2O \rightarrow \left(n + \frac{m}{2}\right)H_2 + nCO$ (3)

Water gas shift: $CO + H_2O \leftrightarrow H_2 + CO_2$ (4)

Boudouard reaction: $C + CO_2 \rightarrow 2CO$ (5)

3.3. Extractives yields

Total amounts of extractives are shown in Fig. 4. The largest amount of extractives (11 wt%, db) was determined in needles, whereas the extractives content was significantly lower in branches (about 7 wt%, db), corresponding to results of Matisons et al. [67,68].

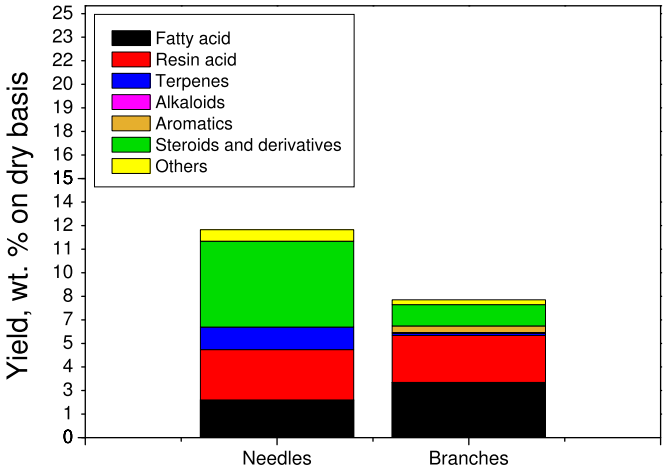

Fig. 4. Yields of non-treated wood fraction extractives. The yields were determined using a Soxhlet apparatus.

The extraction of needles led to significantly greater yields of steroids and terpenes than the extraction of branches. The major compositional difference of pinewood needles to other wood fractions is the high content of terpenes, which are represented by monoterpenes, numerous sesquiterpenes, diterpenoids and their derivatives, as reported previously [69]. The extraction of branches showed a greater yield of fatty acids which were mainly represented by hexadecanoic acids. The pinewood branches can include knots with the high content of resin acids and lignans. However, the content of lignans in branches is essentially lower than in knots [55]. The resin derivatives in branches extractives are mainly represented by the abietane group, as previously detected by Backlund et al. [31].

3.4. Py-GC/MS analysis

The formation of main compounds in needles and branches pyrolysis was investigated by Py-GC/MS. The relative peak areas of 27 identified compounds were categorized as acid, ketone, aldehyde, furan, phenol and other products as shown in Fig. 5. The results

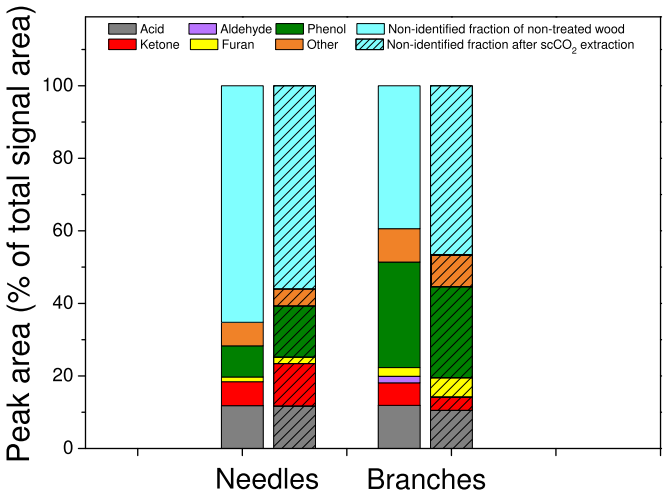

Fig. 5. Relative peak area of volatile products at 600°C using Py-GC/MS shown in % of total chromatographic peak area. The identified peaks are grouped in acid, ketone, aldehyde furan, phenol, other and non-identified product fractions. The results are shown for non-treated wood fraction (plain) and samples after $scCO_2$ extraction (striped pattern).

indicated that the relative compositions of volatiles were nearly similar for all wood fractions. The compounds in pyrolysis vapor are all oxygenated chemicals, due to the large amount of oxygen in biomass. The other identified pyrolysis products are methyl glyoxal, levoglucosan, acetamide, N - methyl - N - [4 - (3 - hydroxypyrrolidinyl) - 2 - butynyl], phorbol, and retinoyl glucuronide. The compounds from functional groups of acids, ketones, and phenols were the dominating products in both non-treated wood fractions and samples after $scCO_2$ extraction. The high concentration of acetic acid was generated from elimination of the acetyl groups originally linked to the xylose unit [70]. Ketone and aldehyde compounds are the main products of secondary volatiles, whose small molecular products were derived from monosaccharides breakdown. The cellulose forms levoglucosan in the first step by the depolymerization, then undergoes dehydration and isomerization reaction to form anhydrosugars [71].

The anhydrosugars further react to form acids, furans, and aldehydes by dehydration, fragmentation and condensation reactions, respectively [72]. The breakdown of glycosidic bonds and the rearrangement of cellulose monomer resulted in the formation of levoglucosan only in potassium lean branches ($K^+ \approx 0.33$ wt%). Interestingly, levoglucosan was not detected in potassium rich needles ($K^+ \approx 1.1$ wt%) during Py/GC–MS analysis [73]. This indicates that potassium plays a minor role on the levoglucosan formation.

3.5. TG-FTIR analysis

The volatiles emitted during the pyrolysis of non-treated needles and branches and samples after $scCO_2$ extraction were characterized by FTIR spectroscopy. The gas concentrations were not quantified.

However, since the FTIR measurements were conducted under similar pyrolysis conditions, the gas release profiles for the different wood fractions were compared. The FTIR spectra of both fractions were recorded at 300°C, corresponding to the average temperature of the primary devolatilization reactions [74],w which are shown in Fig. 6. The condensable gases contain water (4000–3500 cm^{-1}, 1900–1300 cm^{-1}) and primary tars [75]. The water includes both free and bound water. The broad absorption bands (3050–2850 cm^{-1}, 1450–1200 cm^{-1}, 1100–960 cm^{-1}) are characteristic for the absorption of alcohols [51]. The hydroxyl (-OH) region (1300–1000 cm^{-1}) represents the absorption of carboxylic acids, esters, ethers, and alcohols [76]. Light tars containing carboxyl groups such as acetic and formic acid can be formed from the degradation of holocelluloses, and methanol is formed from the methoxy groups (-OCH_3) of lignin [77]. The relative compositions of volatiles were nearly similar for needles and branches forming aldehydes, ketones, acids, and esters between 1900 and 1600 cm^{-1} and acids and aromatics between 1400 and 1200 cm^{-1}. Methane can be

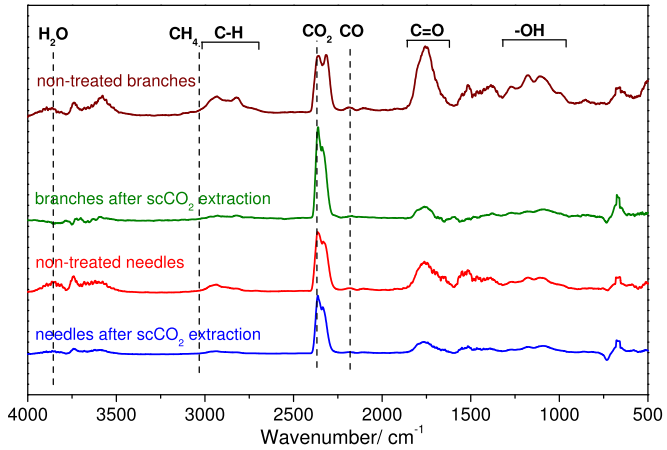

Fig. 6. TG-FTIR of non-treated pinewood fractions and samples after $scCO_2$ extraction.

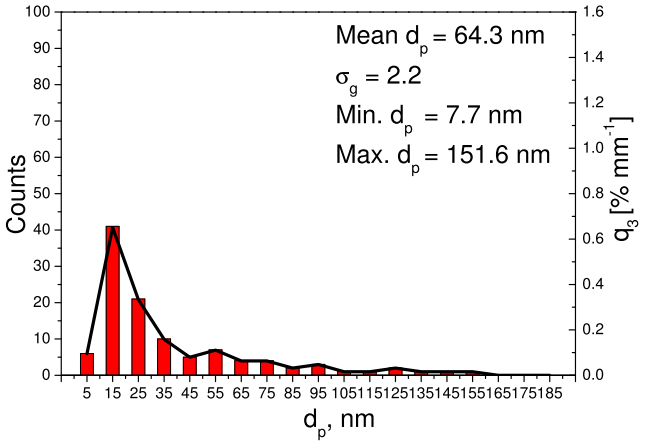

(a): Soot from needles after $scCO_2$

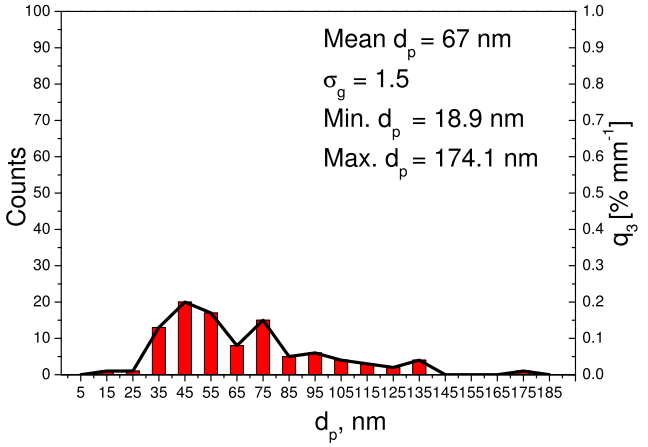

(b): Soot from non-treated branches

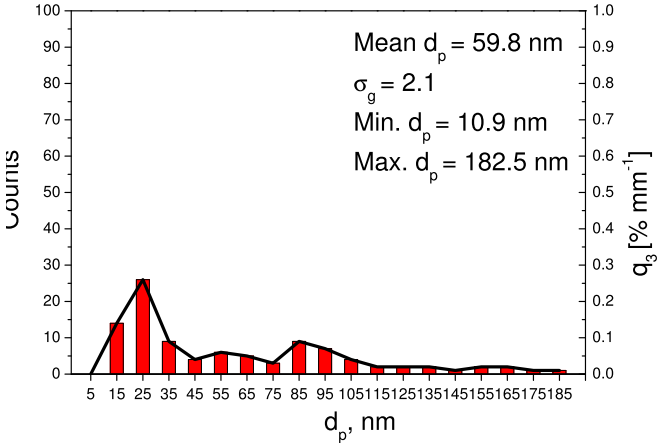

(c): Soot from branches after $scCO_2$

Fig. 7. Particle size distributions of soot from needles and branches after $scCO_2$ extraction and non-treated branches.

formed at temperatures above 600°C [78] by the cracking of weakly bonded methoxy groups [79]. The TG-FTIR band of non-treated wood fractions showed an absorption band of methane between 3150 and 2850 cm^{-1}, whereas this band is not present during TG-FTIR analysis of wood fractions from $scCO_2$ extraction. The results indicate that the weak methoxy groups were removed by the supercritical $scCO_2$ pretreatment at temperatures below 530°C, as shown in the supplemental

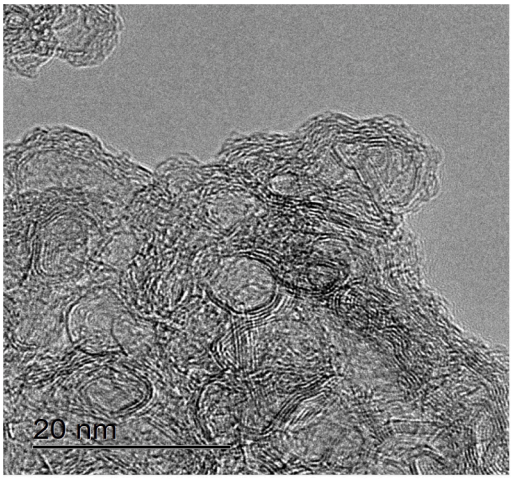

(a): Non-treated needles soot

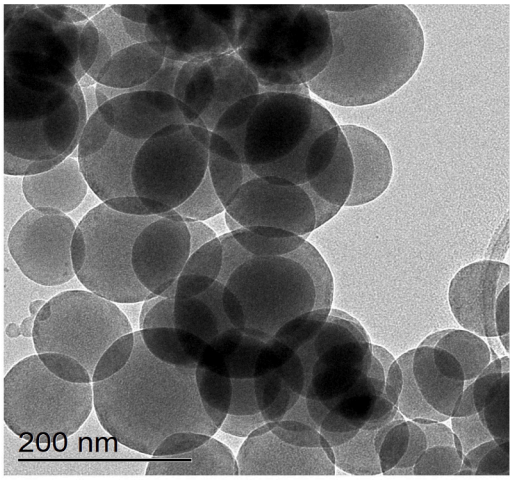

(b): $ScCO_2$ extracted branches soot

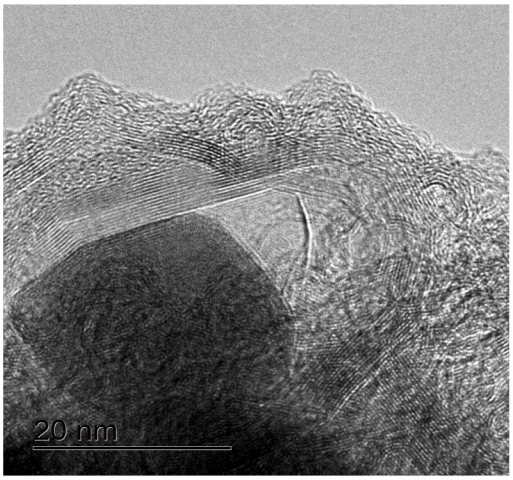

(c): Non-treated needles soot

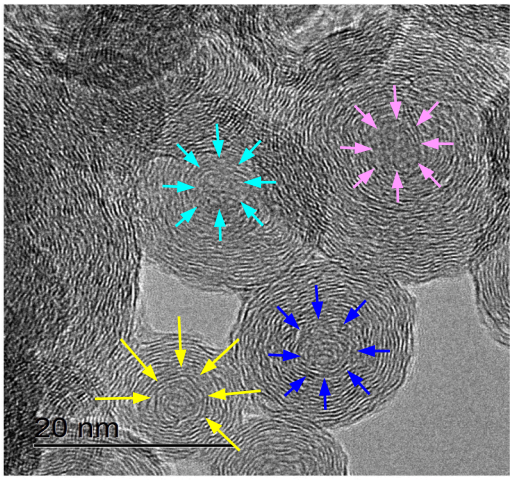

(d): $ScCO_2$ extracted needles

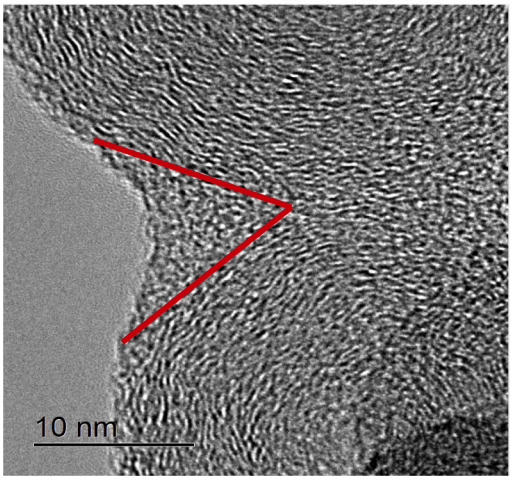

(e): Non-treated branches soot

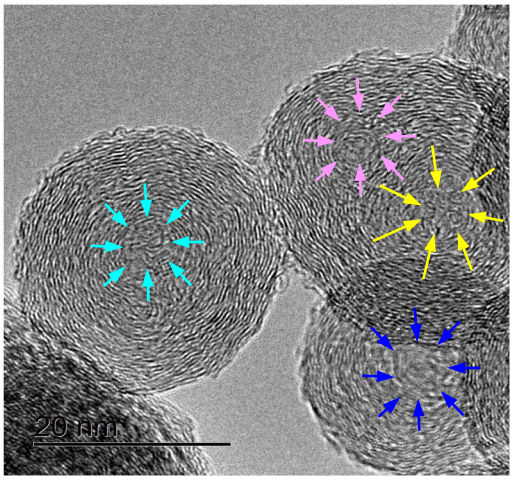

(f): $ScCO_2$ extracted branches soot

Fig. 8. TEM images of soot generated from non-treated needles and branches and samples after $scCO_2$ extraction. In (d) and (f) the arrows indicate the soot particle cores. In (e) the red lines indicate a separation of two different carbon structures. (For interpretation of the references to colour in this figure legend, the reader is referred to the web version of this article.)

material (Figs. S-4 and S-5).

3.6. Particle size analysis

Fig. 7 contains plots of the size distributions of primary soot particles plotted as fractions of the number of particles in each size range.

The calculated geometric mean diameters varied from 59.8 to 67 nm, and were similar to the values reported for the soot obtained from pyrolysis of wood and wheat straw (30.8–77.7 nm) [43]. The particle size of non-treated soot needles was not possible to determine due to their non-spherical shape. The soot particles after $scCO_2$ extraction of needles and branches appeared to be densely fused together with more irregular edges indicating a similar nanostructure to soot particles from hemicellulose pyrolysis [80].

3.7. Soot nanostructure

The nanostructure of the soot from non-treated needles and branches and $scCO_2$ extracted fractions was studied by TEM. Fig. 8(a), (b) show representative images. In all cases, the soot particles appear as agglomerates, ranging from well-defined primary particles as in $scCO_2$ extracted soot branches to agglomerates with almost non-visible primary particles as in non-treated needles. Primary soot particles exhibited a core-shell structure, with mostly single cores and a low fraction of multiple cores, as shown in Fig. 8(f).

TEM analysis indicates that both the fine and large primary soot particles consisted of graphene sheets, which grow circumferentially from the particle core. At the contact surfaces of these primary particles an almost amorphous structure appears, gluing together these particles, as shown in Fig. 8(e). Fig. 8(d), (f) show that the particle cores consist mainly of randomly oriented and curved graphene layers. Non-treated soot needles do not show the same circumferential structure with a wavy graphitic structure spanning over the whole agglomerate. All soot samples contained two different carbon structures.

The graphene segments of soot from non-treated branches and $scCO_2$ extracted needles and branches were well-ordered and flat with the smaller curvature of an average particle size (0.9–0.98; flat graphene ≈ 1 [81]). Table 4 summarizes the characteristics of different soot samples with regards to single or/and multiple cores, curvature and separation distance of graphene layers. The mean separation distance of soot graphene segments (0.35 nm) was slightly greater than that of graphite (0.335 nm) [82]. The mean separation distance of non-treated soot needles was similar to that of pinewood soot and graphite (0.33 nm) [43]. The non-treated soot needles consisted of the longest graphene segments (13.2 nm) with the lower curvature compared to other soot samples, indicating the arrangement of soot nanostructure in both onion rings and straight ribbon structures.

The results demonstrate that the extractives composition is the main factor influencing the nanostructure of soot. The alkali metal content had less influence on the soot nanostructure due to the small difference in the inorganic composition of raw needles and branches and fractions after $scCO_2$ extraction. Previous studies showed that low separation distances (close to that of graphite) and high periodicity lead to lower oxidation of carbon materials, while the more bent graphene layers might enhance the reactivity [82,83]. Compared to soot from non-treated branches, the non-treated soot from needles pyrolysis showed a more curved structure with the longer graphene layers, indicating either a higher porosity or larger fraction of amorphous carbon [84,85]. Moreover, soot particles from $scCO_2$ extracted needles contained more single core structures than soot from non-treated needles with the less recognizable core. The straight graphene layers of the neighboring soot particles from non-treated needles appear to be merged, forming a continuous surface with a large number of crystallites. The extractives removal from needles led to the formation of a soot nanostructure that is similar to $scCO_2$ extracted soot branches. The greater yields of steroids and terpenes during the $scCO_2$ extraction of needles than during the extraction of branches and the similar nanostructure of soot from extracted needles and branches strongly suggest the influence of extractives on the soot nanostructure. In addition, analysis of extract composition shows that the resin acids and steroids compounds are the most probable cause for the agglomeration due to the presence of double bonds and carbonyl groups. FTIR analysis showed that double bond and carbonyl functional groups were removed during $scCO_2$ extraction and thus, soot particles from $scCO_2$ extracted wood fractions were less agglomerated than those from non-treated wood. The removal of extractives from wood fractions reduced soot agglomeration and decreased particle size of soot, leading to formation of a structure that is similar to fullerene. However, the separation distance of the graphene layers of soot from non-treated samples and $scCO_2$ extracted wood remained similar to graphite (0.335 nm).

3.8. Char and soot reactivity

Fig. 9 shows differential weight loss curves (DTG) for the 40% volume fraction CO_2 gasification of solid residues from pyrolysis of non-treated needle and branch, samples after $scCO_2$ extraction, and microwave char reacted in the drop tube furnace. The DTG curves show a single broad peak in CO_2 gasification, indicating a heterogeneous soot mixture with respect to the composition and particle size as suggested by Russell et al. [86]. The maximal reaction rates of both branches and needles solid fractions varied from 850 to 900°C, whereas the maximum reaction rate of non-treated microwave char was about 140°C less than that of microwave char reacted in the DTF, indicating an increase in the char graphitization with the additional heat treatment.

Overall, the thermogravimetric analysis showed that solid residues collected from pyrolysis of wood fractions after $scCO_2$ were similarly reactive in CO_2 gasification to solid residues generated from non-treated samples. This indicates less significant effect of $scCO_2$ pretreatment on the CO_2 reactivity of solid residues. The maximal reaction rate of both soot and char samples from heat treatment of non-treated

Table 4
Summary of soot characteristics using TEM (core, curvature, separation distance) prepared from non-treated needles and branches and samples after $scCO_2$ extraction.

Soot	Fiber length	Curvature[b]	d_{sep}[a,b]	Core[c,d]
	nm		nm	
Non-treated needles	13.2 ± 7.9	0.7 ± 0.33	0.33 ± 0.01	No clear core
$ScCO_2$ extracted needles	4.1 ± 2.3	0.9 ± 0.01	0.35 ± 0.01	s
Non-treated branches	5.1 ± 2.9	0.87 ± 0.04	0.35 ± 0.01	m & mostly s
$ScCO_2$ extracted branches	5.2 ± 3.5	0.84 ± 0.05	0.35 ± 0.01	m & mostly s

[a] Separation distance.
[b] Calculation of mean curvature and d_{sep} of graphene layers measured only on crystallites.
[c] *s* - single core and
[d] *m* - multiple cores.

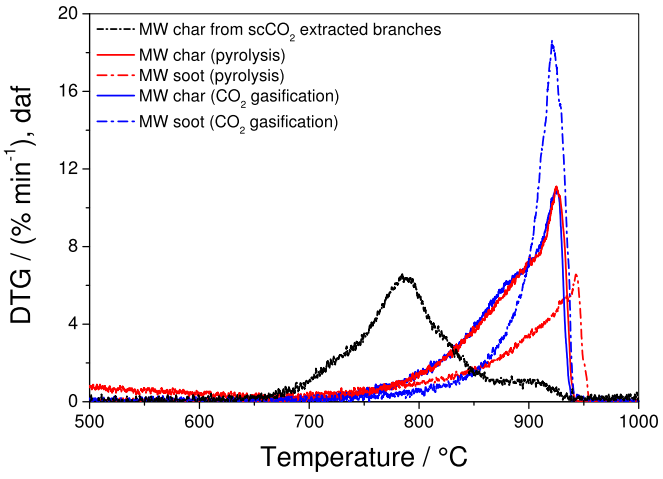

9(a): Microwave reacted char from branches

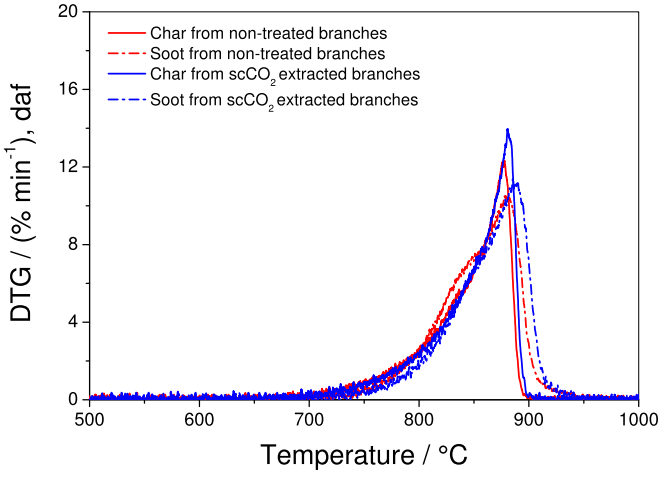

9(b): Branches

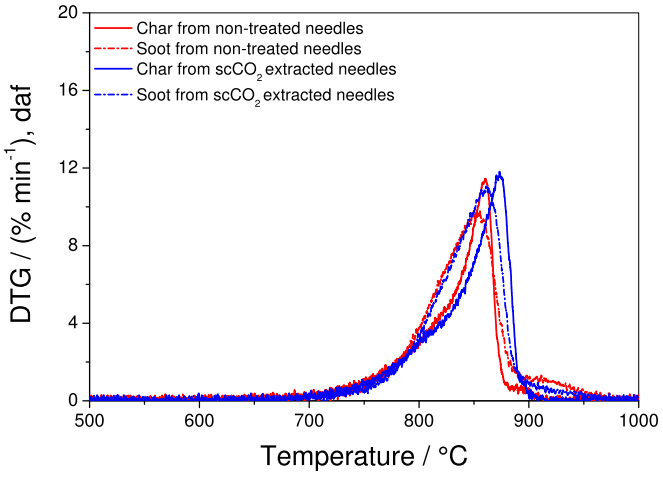

9(c): Needles

Fig. 9. (a)–(c) DTG curves of char and soot from pyrolysis and CO_2 gasification of microwave reacted char and from pyrolysis of non-treated needles and branches and samples after $scCO_2$ extraction reacted in 40% volume fraction CO_2 + 60% volume fraction N_2.

and $scCO_2$ extracted wood fraction of the same origin remained also similar except the solid residues from the microwave pretreatment.

The r_{max} values for the char from pyrolysis or CO_2 gasification of microwave pre-treated branches varied from 1.3 to 1.5 s^{-1}, whereas the r_{max} values for the soot samples generated under similar conditions ranged from 0.6 to 0.7 s^{-1}, corresponding to the previous results [43]. The CO_2 reactivity of both char and soot from microwave pretreated branches and further reacted under pyrolysis and CO_2 gasification in the DTF was almost similar, as shown in the supplemental material (Table S-2). This indicates less influence of the heat treatment atmosphere on the CO_2 reactivity of microwave pretreated feedstocks. The maximal reaction rate of char and soot from needles was almost 80 times greater than that of solid residues from pyrolysis of branches in the drop tube reactor, as shown in the supplemental material (Table S-2). This emphasizes the importance of the feedstock origin on the CO_2 reactivity of soot and char. This study showed that the differences in nanostructure of soot had no influence on the soot reactivity and might be related to the similar separation distance of graphene layers. However, the composition of original feedstock and microwave pretreatment had a stronger influence on the CO_2 reactivity of collected solid residues than the differences in nanostructure, $scCO_2$ extraction and heat treatment atmosphere.

3.9. Process overview

The total yield of products after $scCO_2$ extraction, microwave activation and CO_2 gasification of pinewood branches is shown in Fig. 9. The combination of $scCO_2$ extraction allows 3.6% of extractives to be obtained from branches that can be potentially used for value-added chemicals. In addition, the low temperature microwave activation of $scCO_2$ extracted residue provides a novel route to bio-oil production that can be integrated as a part of biorefinery due to the high yield of liquid products (25.2%). Supercritical carbon dioxide has been demonstrated as an effective solvent for the extraction of several products on an industrial scale including hops, coffee and spices [10]. More recently supercritical extraction with carbon dioxide has been demonstrated to be an effective pre-treatment for biomass prior to downstream processing as part of an integrated biorefinery [4,87]. Economic assessments of such processes have been shown to be commercially viable when used in combination with other biorefinery technologies for the production of value added products. Extraction of wood has been shown to reduce potentially hazardous auto-oxidation that can take place during storage [3,88]. As such, if supercritical extraction could be utilized as part of an integrated biorefinery its application on on a commercial scale could be viable and would lead to the production of valuable additional products (Fig. 10). In contrast, microwaves have for a long time been employed as an effective heating method on an industrial scale for heating in the food industry.

Pilot continual microwave pyrolysis systems already operate at a multiple kg per hour scales and recent studies have explored the potential to scale microwave pyrolysis to an industrial capacity [89]. Although further research is needed to prove the application of microwave pyrolysis and gasification at scale, this technology does offer significant potential to produce higher value bio-products in a shorter residence time when compared to conventional pyrolysis. The combination of supercritical carbon dioxide extraction coupled with microwave pyrolysis would be attractive technologies for valuable chemicals production as part of a future integrated biorefinery.

4. Conclusion

The novelty of this work relies on the fact that the $scCO_2$ extraction of wood increases syngas yield in gasification and generates soot particles with the fullerene-like structure. Optimized extraction conditions based on the amount of fatty and resin acids remaining in the pinewood fractions following supercritical treatment enabled the extraction of

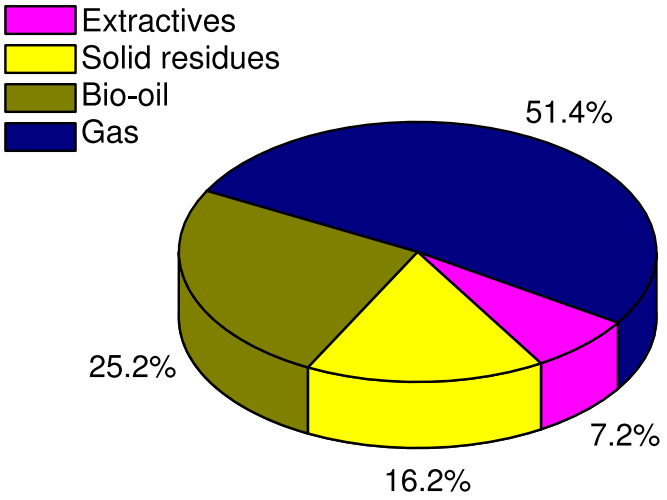

Fig. 10. Total yield of products after $scCO_2$ extraction, microwave pyrolysis and CO_2 gasification of pinewood branches.

more than half of these compounds. Overall, the low temperature microwave activation of $scCO_2$ extracted wood samples provided a novel and energy efficient route to bio-oils and feedstock with excellent properties for gasification. The differences in lignocellulosic composition of wood fractions affected the nanostructure of soot more than the alkali metal content that remained only slightly changed after $scCO_2$ extraction. Therefore, the wood pre-treatment under $scCO_2$ extraction conditions and microwave pyrolysis have potential to increase a syngas production during entrained flow gasification with the minimal influence on the solid product yields and their reactivity in CO_2 gasification.

CRediT authorship contribution statement

Anna Trubetskaya: Conceptualization, Formal analysis, Investigation, Data curation, Writing - original draft, Writing - review & editing, Visualization, Funding acquisition. **Andrew J. Hunt:** Conceptualization, Investigation, Resources, Writing - review & editing, Supervision, Funding acquisition. **Vitaliy L. Budarin:** Conceptualization, Formal analysis, Funding acquisition. **Thomas M. Attard:** Software, Validation, Formal analysis, Data curation, Writing - review & editing. **Gerrit R. Surup:** Software, Writing - original draft. **Mehrdad Arshadi:** Methodology, Validation, Resources, Project administration, Funding acquisition. **Kentaro Umeki:** Methodology, Resources, Supervision, Funding acquisition.

Declaration of competing interest

None.

Acknowledgements

The authors gratefully acknowledge financial support from FORMAS (CETEX project), Kempe Foundation, Björn Wahlströms, and Jernkontoret Stiftelsen. TEM work was performed at DTU Danchip/Cen the National Center for Micro and Nanofabrication at the Technical University of Denmark. We acknowledge Dr. Daniel Eriksson from Swedish Academy of Agricultural Sciences in Umeå for the preparation of pinewood fractions. Dr. Andrew Hunt would like to acknowledge the financial support of the Thailand Research Fund (RSA6280031) and Khon Kaen University. Financial support from the Center of Excellence for Innovation in Chemistry (PERCH-CIC), Ministry of Higher Education, Science, Research and Innovation is gratefully acknowledged. All authors have read and agreed to the published version of the manuscript

Appendix A. Supplementary data

Supplementary data to this article can be found online at https://doi.org/10.1016/j.fuproc.2020.106633.

References

[1] T.M. Attard, N. Bukhanko, D. Eriksson, M. Arshadi, P. Geladi, et al., Supercritical extraction of waxes and lipids from biomass: a valuable first step towards an integrated biorefinery, J. Clean. Prod. 177 (2018) 684–698.
[2] E. Boren, L. Pommer, A. Nordin, S.H. Larsson, Off-gassing from pilot-scale torrefied pine chips: impact of torrefaction severity, cooling technology, and storage times, Fuel Process. Technol. 202 (2020) 106380.
[3] M. Arshadi, A.J. Hunt, J.H. Clark, Supercritical fluid extraction (SFE) as an effective tool in reducing auto-oxidation of dried pine sawdust for power generation, RSC Adv. 2 (2012) 1806–1809.
[4] T.M. Attard, M. Arshadi, C. Nilsson, V.L. Budarin, E. Valencia-Reyes, J.H. Clark, et al., Impact of supercritical extraction on solid fuel wood pellet properties and off-gassing during storage, Green Chem. 18 (2016) 2682–2690.
[5] V.L. Budarin, P.S. Shuttleworth, J.R. Dodson, A.J. Hunt, B. Lanigan, R. Marriott, et al., Use of green chemical technologies in an integrated biorefinery, Energy Environ. Sci. 4 (2011) 471–479.
[6] S.M. Smith, E. Sahle Demessie, J.J. Morrell, K.L. Levien, H. Spliethoff, H. Ng, Supercritical fluid (SCF) treatment: its effect on bending strength and stiffness of ponderosa pine sapwood, Wood Fiber Sci. 25 (1993) 119–123.
[7] C.G. Pereira, M.A.A. Meireles, Economic analysis of rosemary, fennel and anise essential oils obtained by supercritical fluid extraction, Flav. Fragr. J. 22 (2007) 407–413.
[8] F. Chemat, M. Abert Vian, G. Cravotto, Green extraction of natural products: concept and principles, Int. J. Mol. Sci. 13 (2012) 8615–8627.
[9] H.A. Ruiz, R.M. Rodriquez-Jasso, B.D. Fernandes, A.A. Vicente, J.A. Teixeira, Hydrothermal processing, as an alternative for upgrading agriculture residues and marine biomass according to the biorefinery concept: a review, Renew. Sust. Energ. Rev. 21 (2013) 35–51.
[10] A.J. Hunt, E.H.K. Sin, R. Marriott, J.H. Clark, Generation, capture, and utilization of industrial carbon dioxide, ChemSusChem 3 (2010) 306–322.
[11] E.H.K. Sin, R. Marriott, A.J. Hunt, J.H. Clark, Identification, quantification and chrastil modelling of wheat straw wax extraction using supercritical carbon dioxide, C. R. Chim. 17 (2014) 293–300.
[12] G. Brunner, An Introduction to Fundamentals of Supercritical Fluids and the Application to Separation Processes, Springer, 1994.
[13] G. Brunner, Supercritical fluids: Technology and application to food processing, J. Food Eng. 67 (2005) 21–33.
[14] J. Wang, H. Cui, S. Wei, S. Zhuo, L. Wang, Z. Li, et al., Separation of biomass pyrolysis oil by supercritical CO_2 extraction, Smart Grid Renew. Energy 1 (2010) 98–107.
[15] J.L. Goldfarb, L. Buessing, E. Gunn, M. Lever, A. Billias, E. Casoliba, et al., Novel integrated biorefinery for olive mill waste management: utilization of secondary waste for water treatment, ACS Sustain. Chem. Eng. 5 (2017) 876–884.
[16] A. Schievano, F. Adani, L. Buessing, A. Botto, E.N. Casoliba, M. Rossoni, et al., An integrated biorefinery concept for olive mill waste management: supercritical CO_2 extraction and energy recovery, Green Chem. 17 (2015) 2874–2887.
[17] M. Miura, H. Kaga, T. Yoshida, K. Ando, Microwave pyrolysis of cellulosic materials for the production on anhydrosugars, J. Wood Sci. 47 (2001) 502–506.
[18] R. Ruan, P. Chen, R. Hemmingsen, V. Morey, D. Tiffany, Size matters: small distributed biomass energy production systems for economic viability, Int. J. Agric. Biol. Eng. 1 (2008) 64–68.
[19] D. Neves, H. Thunman, A. Matos, L. Tarelho, A. Gomez-Barea, Characterization and prediction of biomass pyrolysis products, Prog. Energy Combust. Sci. 37 (2011) 611–630.
[20] A. Trubetskaya, P. Glarborg, A.D. Jensen, P.A. Jensen, A.D. Garcia, K. Umeki, Effect of fast pyrolysis conditions on biomass solid residues at high temperatures, Fuel Process. Technol. 143 (2016) 118–129.
[21] M.J. Gronnow, R.J. White, J.H. Clark, D.J. Macquarrie, Energy efficiency in chemical reactions: a comparative study of different reaction techniques, Org. Process. Res. Dev. 9 (2005) 516–518.
[22] A. Dominguez, J.A. Menendez, Y. Femandez, J.M.V. Nabais, P.J.M. Carrott, M.M.L.R. Carrott, Conventional and microwave pyrolysis of coffee hulls for the production of a hydrogen rich fuel gas, J. Anal. Appl. Pyrolysis 79 (2007) 128–135.
[23] F. Yu, S. Deng, P. Chen, Y. Liu, Y. Wan, A. Olson, et al., Physical and chemical properties of bio-oils from microwave pyrolysis of corn stover, Appl. Biochem. Biotechnol. 137 (2007) 597–970.
[24] V.L. Budarin, J.H. Clark, B.A. Lanigan, P. Shuttleworth, D.J. Macquarrie, Microwave assisted decomposition of cellulose: a new thermochemical route for biomass exploitation, Bioresour. Technol. 101 (2010) 3776–3779.
[25] R.C. Pettersen, The Chemical Composition of Wood, Adv Chem 207 (1984) 57–126.
[26] G. Gustafsson, Heartwood and Lightwood Formation in Scots Pine – A Physological Approach, PhD thesis Swedish University of Agricultural Sciences, 2001.
[27] J. Werkelin, B.J. Skrifvars, M. Zevenhoven, B. Holmbom, M. Huppa, Chemical forms of ash-forming elements in woody biomass fuels, Fuel 89 (2010) 481–493.
[28] A. Oasmaa, E. Kuoppala, S. Gust, Y. Solantausta, Fast pyrolysis of forestry residue. 1. Effect of extractives on phase separation of pyrolysis liquids, Energy Fuel 17 (2003) 437–443.
[29] S. Myeong, S.H. Han, S.J. Shin, Analysis of chemical compositions and energy

contents of different parts of yellow poplar for development of bioenergy technology, J. Korean. For. Soc. 99 (2010) 706–710.
[30] P. Hakkila, Utilization of Residual Biomass, Springer, 1989.
[31] I. Backlund, Cost-effective Cultivation of Lodgepole Pine for Biorefinary Applications, PhD thesis Swedish University of Agricultural Sciences, 2013.
[32] P. Koch, Lodgepole pine in North America: nonwood products characterization of tree parts, For. Prod. Soc. 2 (1996) 1–417.
[33] G.R. Surup, A.J. Hunt, A. Attard, V.L. Budarin, M. Arshadi, A. Trubetskaya, et al., The effect of wood composition and supercritical CO_2 extraction on charcoal production in ferroalloy industries, Energy 193 (2019) 116696.
[34] L. Bilali, M. Benchanaa, K. El Harfi, A. Mokhlisse, A. Outzourhit, A detailed study of the microwave pyrolysis of the Moroccan (Youssoufia) rock phosphate, J. Anal. Appl. Pyrolysis 73 (2005) 1–15.
[35] J.A. Menendez, A. Dominguez, Y. Fernandez, J.J. Pis, Evidence of self-gasification during the microwave-induced pyrolysis of coffee hulls, Energy Fuel 21 (2007) 373–378.
[36] C. Wu, V. Budarin, M. Wang, M.J. Gronnow, Y. Wu, P.T. Williams, et al., CO_2 gasification of biochar derived from conventional and microwave pyrolysis, J. Anal. Appl. Pyrolysis 157 (2015) 533–539.
[37] C. Wu, V.L. Budarin, M.J. Gronnow, M. De Bruyn, J.A. Onwudili, J.H. Clark, et al., Conventional and microwave-assisted pyrolysis of biomass under different heating rates, J. Anal. Appl. Pyrolysis 107 (2014) 276–283.
[38] S.S. Lam, H.A. Chase, A Review on waste to energy processes using microwave pyrolysis, Energies 5 (2012) 4209–4232.
[39] C.R. McElroy, T.M. Attard, T.J. Farmer, D. Gaczynski, D. Thornthwaite, J.H. Clark, et al., Valorization of spruce needle waste via supercritical extraction of waxes and facile isolation of nonacosan-10-ol, J. Clean. Prod. 171 (2018) 557–566.
[40] M. Arshadi, R. Gref, Emission of volatile organic compounds from softwood pellets during storage, For. Prod. J. 55 (2005) 132–135.
[41] V. Abdelsayed, C.R. Ellison, A. Trubetskaya, M.W. Smith, D. Shekhawat, Effect of microwave and thermal pyrolysis of low-rank and pine wood on product distributions and char structure, Energy Fuel 33 (2019) 7069–7082.
[42] C. Wu, D. Lisha, J. Onwudili, P.T. Williams, J. Huang, Effect of Ni particle location within the mesoporous MCM-41 support for hydrogen production from the catalytic gasification of biomass, ACS Sust. Chem. Eng. 1 (2013) 1083–1091.
[43] A. Trubetskaya, P.A. Jensen, A.D. Jensen, A.D. Garcia Llamas, K. Umeki, D. Gardini, et al., Effects of several types of biomass fuels on the yield, nanostructure and reactivity of soot from fast pyrolysis at high temperatures, Appl. Energy 171 (2016) 468–482.
[44] A. Bach-Oller, K. Umeki, E. Furusjö, On the role of potassium as a tar and soot inhibitor in biomass gasification, Appl. Energy 254 (2019) 113488.
[45] A. Trubetskaya, K. Umeki, M.T. Timko, Prediction of fast pyrolysis products yields using lignocellulosic compounds and ash contents, Appl. Energy 257 (2020) 113897.
[46] A. Zolin, A.D. Jensen, P.A. Jensen, K. Dam-Johansen, Experimental study of char thermal deactivation, Fuel 81 (2002) 1065–1075.
[47] G.R. Surup, A. Trubetskaya, H. Nielsen, T. Vehus, P.A. Eidem, Characterization of renewable reductants and charcoal-based pellets for the use in ferroalloy industries, Energy 167 (2019) 337–345.
[48] A. Trubetskaya, K. Umeki, N. Souhi, Categorization of tars from fast pyrolysis of pure lignocellulosic compounds at high temperature, Renew. Energy 141 (2019) 751–759.
[49] A.W. Coats, J.P. Redfern, Kinetic parameters from thermogravimetric data, Nature 201 (1964) 68–69.
[50] K. Qin, Entrained Flow Gasification of Biomass, PhD thesis Technical University of Denmark, 2012.
[51] K. Werner, L. Pommer, M. Broström, Thermal decomposition of hemicelluloses, J. Anal. Appl. Pyrolysis 110 (2014) 130–137.
[52] W.S. Rasband, J. Image, U.S. National Institutes of Health: Bethesda, MD, http://imagej.nih.gov/ij, (2012).
[53] E. Cenker, G. Bruneaux, T. Dreier, C. Schulz, Determination of small soot particles in the presence of large ones from time-resolved laser-induced incandescence, Appl. Phys. B Lasers Opt. 118 (2015) 169–183.
[54] A. Sluiter, B. Hames, R. Ruiz, C. Scarlata, J. Sluiter, D. Templeton, et al., Determination of Structural Carbohydrates and Lignin in Biomass. Golden (CO): National Renewable Energy Laboratory; Report No. NREL/TP-510-42618, Contract No.: DE-AC36-08-GO28308 (July 2011).
[55] S. Willför, J. Hemming, A.S. Leppänen, Analysis of Extractives in Different Pulps - Method Development, Evaluation, and Recommendations, Åbo Akademi University, Finland, 2004–2009 Laboratory of Wood and Paper Chemistry; Report No. B1 of the EU COST E41 action “Analytical tools with applications for wood and pulping chemistry”.
[56] B. Hames, R. Ruiz, C. Scarlata, J. Sluiter, A. Sluiter, Preparation of Samples for Compositional Analysis, National Renewable Energy Laboratory, Golden (CO), June 2011 Report No. NREL/TP-510-42620. Contract No.: DE-AC36-99-GO10337.
[57] K. Thammasouk, D. Tandjo, M.H. Penner, Influence of extractives on the analysis of herbaceous biomass, J. Agric. Food Chem. 45 (1997) 437–443.
[58] R. Moya, A. Rodriguez-Zuniga, A. Puente-Urbina, Thermogravimetric and devolatilization analysis for five plantation species: effect of extractives, ash composition, chemical compositions and energy parameters, Thermochim. Acta 647 (2017) 36–46.
[59] H. Yang, R. Yan, H. Chan, D.H. Lee, C. Zheng, Characteristics of hemicellulose, cellulose and lignin pyrolysis, Fuel 86 (2007) 1781–1788.
[60] X.J. Guo, S.R. Wang, K.G. Wang, Q. Liu, Z.Y. Luo, Influence of extractives on mechanism of biomass pyrolysis, J. Fuel Chem. Technol. 38 (2010).
[61] J. Lee, X. Yang, H. Song, Y.S. Ok, E.E. Kwon, Effects of carbon dioxide on pyrolysis of peat, Energy 120 (2017) 929–936.
[62] K. Umeki, K. Kirtania, A. Bach-Oller, E. Furusjö, G. Häggström, Reduction of tar and soot formation from entrained-flow gasification of woody biomass by alkali impregnation, Energy Fuel 31 (2017) 5104–5110.
[63] A. Trubetskaya, H. Lange, U. Rova, L. Matsakas, C. Crestini, J.J. Leahy, et al., Structural and thermal characterization of novel organosolv lignins from wood and herbaceous sources, Processes 8 (2020) 1–19.
[64] C. Roy, H. Pakdel, D. Brouillard, The role of extractives during vacuum pyrolysis of wood, J. Appl. Polym. Sci. 41 (1990) 337–348.
[65] G.I. Tingey, Kinetic of the water-gas equilibrium reaction. I. The reaction of carbon dioxide with hydrogen, J. Phys. Chem. 70 (1966) 1406–1412.
[66] H.C. Butterman, M.J. Castaldi, CO_2 as carbon neutral fuel source via enhanced biomass gasification, Environ. Sci. Technol. 43 (2009) 9030–9037.
[67] D. Bergström, M. Matisons, Efficient forest biomass supply chain management for biorefineries, Sveriges lantbrukuniversitet, Sweden, Umeå, 2014 Rapport No. 18-2014.
[68] A. Kilic, H. Hafizoglu, H. Sivrikaya, M. Reunanen, I. Tümen, J. Hemming, et al., Extractives in the cones of Pinus species, Eur. J. Wood Prod. 69 (2011) 37–40.
[69] N. Bukhanko, T. Attard, M. Arshadi, A.J. Hunt, U. Bergsten, J. Clark, et al., Extraction of cones, branches, needles and bark from Norway spruce (*Picea acies*) by supercritical carbon dioxide and soxhlet extractions techniques, Ind. Crop. Prod. 145 (2020) 1–11.
[70] D. Güllü, A. Demirbas, Biomass to methanol via pyrolysis process, Energy Conv. Manage. 42 (2001) 1349–1356.
[71] H. Yuan, S. Xing, H. Li, T. Lu, Y. Chen, Influences of copper on the pyrolysis process of demineralized wood dust through thermogravimetric and Py-GC/MS analysis, J. Anal. Appl. Pyrolysis 112 (2015) 325–332.
[72] Y.C. Lin, J. Cho, G.A. Tompsett, P.R. Westmoreland, G.W. Huber, Kinetics and mechanism of cellulose pyrolysis, J. Phys. Chem. 113 (2009) 20097–20107.
[73] L. Schwarzer, Z. Sarossy, P.A. Jensen, P. Glarborg, J.K. Holm, K. Dam-Johansen, et al., Kinetic parameters for biomass under self-ignition conditions: low-temperature oxidation and pyrolysis, Energy Fuel 33 (2019) 8606–8619.
[74] T. Fisher, M. Hajaligol, B. Waymack, D. Kellogg, Pyrolysis behavior and kinetics of biomass derived materials, J. Anal. Appl. Pyrolysis 62 (2002) 331–349.
[75] Y. Zhang, Z.B. He, L. Xue, D.M. Chu, J. Mu, Influence of a urea - formaldehyde resin adhesive on pyrolysis characteristics and volatiles emission of poplar particleboard, RSC Adv. 6 (2016) 12850–12861.
[76] J. Barton-Pudlik, K. Czaja, Conifer needles as thermoplastic composite fillers: structure and properties, BioResources 11 (2016) 6211–6231.
[77] K. Han, S. Niu, C. Lu, Experimental study on biomass advanced reburning for nitrogen oxides reduction, Process. Saf. Environ. Protect. 88 (2010) 425–430.
[78] N.B. Gao, A.M. Li, C. Quan, L. Du, Y. Duan, TGA-FTIR Py-GC/MS analysis on pyrolysis and combustion of pine sawdust, J. Anal. Appl. Pyrolysis 100 (2013) 26–32.
[79] F. Patuzzi, T. Mimmo, S. Cesco, A. Gasparella, M. Baratieri, Common reeds (*Phragmites australis*) as sustainable energy source: experimental and modelling analysis of torrefaction and pyrolysis processes, GCB Bioenergy 5 (2013) 367–374.
[80] A. Trubetskaya, A. Brown, G.A. Tompsett, M.T. Timko, K. Umeki, J. Kling, et al., Characterization and reactivity of soot from fast pyrolysis of lignocellulosic compounds and monolignols, Appl. Energy 212 (2018) 1489–1500.
[81] J.O. Müller, D.S. Su, U. Wild, R. Schlögl, Bulk and surface structural investigations of diesel engine soot and carbon black, Phys. Chem. Chem. Phys. 9 (2007) 4018–4025.
[82] A. Liati, P.D. Eggenschwiler, D. Schreiber, V. Zelenay, M. Ammann, Variations in diesel soot reactivity along the exhaust after-treatment system, based on the morphology and nanostructure of primary soot particles, Combust. Flame 160 (2013) 671–681.
[83] R.H. Hurt, Structure, properties, and reactivity of solid fuels, 27th Symposium on Combust, 1998, pp. 2887–2904.
[84] R.E. Franklin, Crystallite growth in graphitizing and non-graphitizing carbons, Proc. R. Soc. Lond. Ser. Math. Phys. Eng. Sci. 209 (1951) 196–218.
[85] E. Bar-Zic, A. Zaida, P. Salatino, O. Senneca, Diagnostics of carbon gasification by Raman microprobe spectroscopy, Proc. Combust. Inst. 28 (2000) 2369–2374.
[86] N.V. Russell, T.J. Beeley, C.K. Man, J.R. Gibbins, J. Williamson, Development of TG measurements of intrinsic char combustion reactivity for industrial and research purposes, Fuel Process. Technol. 57 (1998) 113–130.
[87] T.M. Attard, C.R. McElroy, A.J. Hunt, Economic assessment of supercritical CO_2 extraction of waxes as part of a maize stover biorefinery, Int. J. Mol. Sci. 16 (2015) 17546–17564.
[88] T.M. Attard, C.R. McElroy, J.M. Gammons, J.M. Slattery, N. Supanchaiyamat, A.J. Hunt, et al., Supercritical CO_2 extraction as an effective pre-treatment step for wax extraction in a miscanthus biorefinery, ACS Sustain. Chem. Eng. 4 (2016) 5979–5988.
[89] D. Beneroso, T. Monti, E.T. Kostas, J. Robinson, Microwave pyrolysis of biomass for bio-oil production: scalable processing concepts, Chem. Eng. J. 316 (2017) 481–498.